Experimental Thermal and Fluid Science 64 (2015) 13–22

Contents lists available at ScienceDirect

Experimental Thermal and Fluid Science

journal homepage: www.elsevier.com/locate/etfs

Effects of heat flux, mass flux and channel size on flow boiling performance of reentrant porous microchannels

Daxiang Deng [a,b,*], Ruxiang Chen [c], Hao He [d], Junyuan Feng [d], Yong Tang [d], Wei Zhou [a]

[a] Department of Mechanical & Electrical Engineering, Xiamen University, Xiamen 361005, China
[b] ShenZhen Research Institute of Xiamen University, ShenZhen 518057, China
[c] ABB Xiamen Low Voltage Equipment Company, 12-20 Chuangxin 3rd Road, Xiamen 361006, China
[d] Key Laboratory of Surface Functional Structure Manufacturing of Guangdong High Education Institutes, School of Mechanical and Automotive Engineering, South China University of Technology, Guangzhou 510640, China

ARTICLE INFO

Article history:
Received 19 October 2014
Received in revised form 8 January 2015
Accepted 26 January 2015
Available online 4 February 2015

Keywords:
Microchannels
Flow boiling
Reentrant
Channel size

ABSTRACT

Flow boiling within advanced microchannel heat sinks provides efficient and attractive solutions for the cooling of heat-heat-flux devices. In this study, a type of porous-based microchannels with reentrant configurations is developed and tested in heat sink cooling systems. The reentrant porous microchannels (RPMs), which are constructed by porous copper powder, are fabricated by solid-state sintering method under the replication of specially designed sintering modules. Three reentrant porous microchannels with hydraulic diameters of 671 μm,786 μm and 871 μm are tested under boiling deionized water conditions at inlet temperatures of 90 °C, mass flux of 160–300 kg/m^2 s. The effects of heat flux, mass flux and channel size on the flow boiling performance of reentrant porous microchannels are examined. Test results show that the two-phase heat transfer performance of RPMs was strongly dependent on the heat flux, but showed a weak dependence on the mass flux. Reentrant porous microchannels with the medium size were found to enhance two-phase heat transfer rate compared to the other two samples at moderate to high heat fluxes.

1. Introduction

Microchannel heat sinks undergoing two-phase flow boiling offer very high heat transfer rates and simultaneously maintain relatively uniform wall temperatures, thus a large number of research efforts have been taken to implement them in the cooling of microelectronic and military systems [1,2]. To date, solid microchannels such as silicon [3], copper [4], aluminum [5] microchannel heat sinks have been extensively investigated. They are normally of circular (micro tubes) [6], rectangular [7,8], triangular [9] or trapezoidal [10] shapes. However, for all the above microchannels, the bubble nucleation at the incipience of boiling flow is limited by the smooth surface of microchannels, which induces large wall superheat to trigger flow boiling in microchannels. This, evidently, is problematic for the safe operation of microchannel heat sink cooling systems. To address this issue, researchers have attempted to develop more sophisticated means, such as drilling holes [11], adding sprayed ABM coating [12], nano coatings [13,14], diffusion-brazed wire mesh screens [15], sintered porous powder coating [16,17] on the bottom wall, and artificial reentrant cavities [18,19] on the side wall of microchannels. Since the introduction of porous coatings and reentrant cavities extends the surface area notably and increases the nucleation site densities significantly, enhanced flow boiling heat transfer has been reached in such advanced microchannel heat sinks. However, there are critical challenges for the implementation of porous layers, nanocoatings and artificial micro cavities on the microchannel surface after the formation of microchannel base. Meanwhile, these methods apparently increase the fabrication procedure and cost significantly. Furthermore, the nano or porous coatings may separate from the microchannel base wall after long time runs and the merit of porous surfaces may disappear over time [13]. In view of this, a different means, i.e., a novel type of reentrant porous microchannels has been preliminarily developed using the solid-state sintering method by the authors [20]. Other than just by the alteration of microchannel bottom surface or side wall, the reentrant porous microchannels (RPMs) were constructed totally by sintered copper powder, and the reentrant shape was formed by the replication of a Ω-shaped module. Flow boiling tests have demonstrated a significant increase of nucleation sites and therefore a drastic decrease of wall superheat for the onset of nucleate boiling (ONB) compared to

* Corresponding author at: Tel./fax: +86 592 2186383.
E-mail address: dengdaxiang88@gmail.com (D. Deng).

http://dx.doi.org/10.1016/j.expthermflusci.2015.01.015
0894-1777/

Nomenclature

A_c	cross-section area of microchannels, m^2
A_{ch}	total heat transfer area of microchannels, m^2
$A_{c,s}$	cross-sectional area of a single reentrant microchannels, m^2
A_t	platform area of copper block, m^2
d	powder particle diameter, um
D_h	hydraulic diameter, mm
G	mass flux, kg/m^2 s
H_{slot}	height of slot, mm
h_{fg}	latent heat of vaporization, kJ/kg
h_{tp}	local two-phase heat transfer coefficient, kW/m^2 K
k_{Cu}	thermal conductivity of copper block, W/m K
k_{por}	thermal conductivity of reentrant porous microchannels, W/m K
k_s	thermal conductivity of solder, W/m K
L	length of heat sink, mm
L_i	distance from the inlet to thermocouple location in the downstream direction, m
l_{Cu}	distance between the thermocouple and the top surface of copper block, m
l_{hs}	distance between heat sink bottom surface and the bottom of circular portion of reentrant cavity, m
m	fin parameter
$\dot{m}$	mass flow rate, (kg/s)
N	number of reentrant microchannels
ONB	onset of nucleation boiling
P_{cir}	perimeter of circular portion of reentrant microchannel, m
P_{in}	inlet pressure, kPa
Q	total power input, W
q_{eff}	effective heat absorption, W
q''_{eff}	effective heat flux based on platform area, kW/m^2
r	radius of the circular cavity, μm
T_{tci}	thermocouple reading (i = 1–5), °C
T_{in}	inlet fluid temperature, °C
$T_{w,\ tci}$	channel bottom wall temperature at thermocouple location, °C
$\Delta T_{sct,tci}$	wall superheat, °C
$T_{sat,\ tci}$	local saturation temperature of thermocouple location, °C
$\dot{V}$	volumetric flow rate, m^3/s
w	width of the slot, mm
W_{fin}	width of fin between two reentrant microchannels, mm
W_{slot}	width of slot, mm
x	thermodynamic quality

Greek symbols

ε	porosity
η	fin efficiency
θ	arc angle of the circular cavity
φ	heat transfer ratio
ρ	density of fluid, kg/m^3
σ	standard deviation

Subscripts

cir	circular portion
Cu	copper
hs	heat sink
fin	fin
tci	thermocouple location
in	inlet
por	porous
sat	saturation
slot	slot
s	solder
tp	two-phase

solid copper microchannels with the same reentrant configurations. Moreover, significant enhancement of flow boiling heat transfer and mitigation of two-phase instabilities have been achieved.

In conventional solid microchannels, the effects of heat flux and mass flux on their heat transfer performance have been extensively investigated [6–9]. Nevertheless, the knowledge on the flow boiling performance of porous-based microchannels are very limited [20]. On the other side, the microchannel size has been also found to play an important role on the flow boiling performance by many researcher groups [21–25]. Saitoh et al. [21] preformed boiling tests of R-134a in three tubes with diameter of 0.51, 1.12 and 3.1 mm. The results showed that with the decrease of tube diameter, the effect of mass flux on the local heat transfer coefficient decreased, and the two-phase heat transfer performance tended to decrease as well. Lee et al. [22] accessed the effect of microchannel height on nucleation-site activities and bubble dynamics in rectangular silicon microchannels with the widths ranging from 150 to 9000 μm and heights ranging from 5 to 510 μm. Three fluids (water, methanol, and ethanol) tests all demonstrated the bubble nucleation activities were dependent on the microchannel height. Lee and Mudawar [23] explored the influences of hydraulic diameter and width of copper rectangular microchannels on the subcooled boiling performance of microchannels heat sinks. Two-phase heat transfer was found to increase with the hydraulic diameter increasing from 175.7 μm to 334.1 μm, while it deteriorated apparently when the size increased further to 415.9 μm. Besides, the critical role of channel cross-section geometry of silicon microchannels on FC-72 boiling performance was systemically examined by Harirchian and Garimella [24,25]. Rectangular microchannels with depths ranging from 100 μm to 400 μm and widths ranging from 100 μm to 5850 μm were prepared. It was found that the nucleate boiling mechanism dominated when the channels cross-section area exceeded a specific value, and the boiling heat transfer coefficients were independent of channel dimensions therein. Below this threshold value, the heat transfer rate increased as the microchannel cross-sectional area decreased. The flow patterns and pressure drop were also dependent on the channel size. Furthermore, the influence of aspect ratio of rectangular silicon microchannels [26] or diverging copper microchannels [27] has also been reported. As enumerated above, the current efforts concerning on the microchannel size effects were devoted to the solid microchannels with conventional shapes. However, as to the authors' best knowledge, the effect of microchannel size on the flow boiling behavior of porous-based microchannels heat sinks has not yet been understood.

In view of the absence of previous studies on the influences of heat flux, mass flux and microchannel size effects on flow boiling performance of porous microchannels heat sinks, the present work is aimed to perform such studies for the purpose of design optimization of reentrant porous microchannels and their implementation in heat sink cooling systems. The present work significantly expands the measurement database available in Ref. [20] by considering reentrant porous microchannels with different size, and

discusses the influence of several parameters such as heat flux, mass flux and hydraulic diameter on two-phase boiling performance of such new type of microchannels. Three reentrant porous microchannels with hydraulic diameters of 671 μm, 786 μm and 871 μm were fabricated. Boiling curves, heat transfer coefficients and two-phase flow instabilities at a range of mass fluxes are presented and compared using the coolant of deionized water.

2. Experiment

2.1. Fabrication of reentrant porous microchannels

The reentrant porous microchannels were designed to be a unique reentrant configuration, as shown in Fig. 1(a). The hydraulic diameter (D_h) of such unique microchannels can be calculated as follows,

$$D_h = \frac{4A_{c,s}}{P} = \frac{4(W_{slot}H_{slot} + r^2\theta/2 + W_{slot}r\cos((2\pi-\theta)/2)/2)}{2H_{slot} + W_{slot} + r\theta} \quad (1)$$

in which $A_{c,s}$ is the cross-sectional area of a single reentrant microchannels, P is wetted perimeter of a microchannel. r, H_{slot}, W_{slot} denotes the radius of circular cavity, the height and width of narrow slot, respectively. θ is the arc angle of circular cavity, which can be expressed as follows,

$$\theta = 2\pi - \arcsin(W_{slot}/2r) \quad (2)$$

From Eq. (1), it can be noted that the radius of the circular cavity, r, plays a dominant role on the hydraulic diameter of reentrant microchannels. Therefore, the variations of circular cavity radius were focused on to access the channel size effects in this study. Three RPMs with the circular cavity radius of 350 μm, 400 μm, 450 μm were designed, and the hydraulic diameters of RCMs were calculated to be 671, 786 and 871 μm, respectively. Other parameters of these three microchannels were shown in Table 1.

The reentrant porous microchannels were fabricated by solid-state sintering of copper powders under the replication of specially designed Ω-shaped sintering molds. The first step is to process the sintering mold by the micro electrical discharge machining (EDM) wire cut. Graphite based mold with convex Ω shape was carefully machined for the ease of demolding after the high temperature sintering, as graphite is inactive with copper powers at high temperatures. Three sintering molds with different convex Ω geometries were prepared. Then the copper powders were filled on the topside of the Ω-shaped mold. Commercial spherical copper powders of purity over 99.5% were employed. A cover and base plate were used to make sure the backside of sintered porous microchannels was flat. Later, sintering of copper powders was implemented in a furnace with a programmable temperature controller for 30–60 min at 950 ± 10 °C under hydrogen reducing atmosphere. Then the sintered copper specimen was demolded along the length direction very carefully, and the reentrant porous microchannels samples were obtained. Details of the fabrication procedures were illustrated in Ref. [20]. As the metallurgical bonding of copper particles occurred during the high-temperature sintering process, the matrix of reentrant porous microchannels was constructed firmly by porous copper powder. Besides, due to the good strength of sintered porous matrix and the large flat top surface of the microchannels, it was found that the reentrant porous microchannels were strong enough to assemble with screws in the test section as described in the subsequent section, and none cracks of porous wall happened during repeated tests. Fig. 1(b)–(d) shows the SEM photographs of these RPMs with different sizes. All the samples were of the width of 20 mm, thickness of 2 mm, and length of 45 mm. They consisted of 14 parallel microchannels. The parameters of these samples were listed in Table 1.

2.2. Experimental setup

A schematic diagram of the experimental test loop is shown in Fig. 2. A magnetic gear pump drives the fully degassed deionized water through the closed loop. The water temperature is adjusted before entering the inlet of test section by a heat exchanger which connects to a constant temperature water bath, and a condenser locating at the downstream of the test section cools the liquid before it enters back to the water tank. A micro turbine type flowmeter monitors the flow rate through the loop. A variac and wattmeter is utilized to supply the heating power. Flow visualizations are conducted using a microscope and a high-speed camera (Fastec HiSpec DVR 2F). All the measurements of temperatures, pressure and mass flow rate are monitored by an Agilent 34970A data acquisition system.

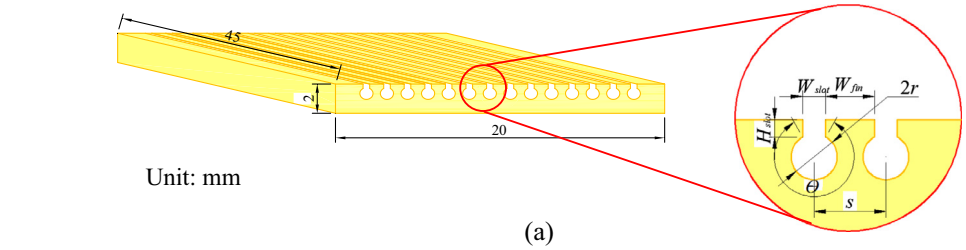

(a)

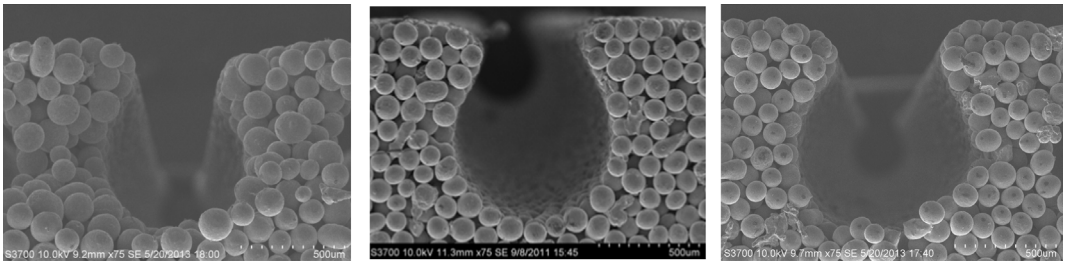

(b) (c) (d)

Fig. 1. Reentrant porous microchannels samples with different sizes: (a) Geometric design of reentrant microchannel; (b) SEM image of the small RPMs with D_h = 671 μm; (c) SEM image of the medium RPMs with D_h = 786 μm; (d) SEM image of the large RPMs with D_h = 871 μm.

Table 1
Specification of the reentrant porous microchannels samples.

Sample	Powder particle size, d (μm)	Porosity of porous matrix, ε	Dimension, $W \times H \times L$ (mm)	Numbers of channels	Hydraulic diameter, D_h (μm)	Cross-section dimension		
						Slot height, H_{slot} (mm)	Slot width, W_{slot} (mm)	Radius of reentrant cavity, r (mm)
RPM-D1	75–110	0.39	20 × 2 × 45	14	671	0.3	0.3	0.35
RPM-D2	75–110	0.39	20 × 2 × 45	14	786	0.3	0.4	0.4
RPM-D3	75–110	0.39	20 × 2 × 45	14	871	0.3	0.4	0.45

The test section, as shown in Fig. 3, consists of the reentrant porous microchannel sample, inlet and outlet plenums, a Pyrex 7740 glass cover plate, an assembling top plate, a fiberglass housing, a copper block heating module and insulating components. Details of the test section construction are available in the previous study [20] with an exploded view, and are not repeatedly presented here. The footprint area of microchannels sample and the top surface of copper block are of the same dimensions, that is, an area of 20 mm × 45 mm. The microchannel sample is soldered on top of the copper block heating module using a thin layer of solder (Pb–Sn–Ag–Sb, k_s = 50 W/m K) to minimize the contact thermal resistance. As the height difference between the flow housing and the top surface of copper block is designed to be 0.1 mm to form a gap to host the solder, it ensures that the solder layer is 0.1 mm thick after the soldering process is completed, and no leakage of solder into the porous microchannels is observed. RTV silicone rubber is utilized in the interface of copper block and flow housing to maintain a leak-proof sealing. Ten cartridge heaters with the maximum total power of 1000 W are utilized to heat the copper block. Five holes with a depth of 10 mm are drilled along the stream-wise direction below the top surface of copper block, and the distance between the centre of holes and the top surface of copper block is designed to be 1.8 mm. Five Type-K shielded thermocouples with a diameter of 1 mm, which have been calibrated in a constant water bath before the test, are embedded to measure the stream-wise temperature distribution in the copper block, i.e., T_{tc1} to T_{tc5} in Fig. 3, which are then utilized to determine the microchannel wall temperature distributions along the flow direction. The locations of these five thermocouples are 2.5 mm, 12.5 mm, 22.5 mm, 32.5 mm, 42.5 mm, respectively, from the channel inlet position, as depicted in Fig. 3. Two Type-K thermocouples are set at about 5 mm before or after the microchannel sample to measure the inlet/outlet temperature. Pressure port spaces are left in the inlet and outlet plenum for the measurement of inlet/outlet pressure by two pressure transducers. Horizontal inlet and outlet manifold arrangements are utilized for the liquid flow, and no deep inlet and outlet reservoirs are adopted to reduce the compressive upstream volume (see Ref. [20] for details). The above means, along with the stiff stainless steel tube to connect the test section and the upstream valve, was expected to provide a means to weaken the two-phase flow instability [28]. A top plate as well as the glass cover above the test piece provide an enclosed passage for the liquid and are sealed with an O-ring. A bakelite insulating block, together with wrapped glass fiber on the side and bottom of test assembly, is used to ensure insulation and minimize heat loss.

The flow boiling tests of reentrant porous microchannels were performed at flow rates of 160–300 kg/m^2 s, and the inlet temperatures were kept at 90 °C, namely, the inlet subcooling of 10 °C. Before each experiment run, the coolant deionized water in the water tank was fully degassed via vigorous boiling for about an hour. Such deaeration means has been also utilized in previous reports [8]. During this process, the vent valve above the reservoir is periodically open to allow dissolved gases to escape to the atmosphere. This also set the test pressure to near atmospheric. During testing, this valve is periodically opened to prevent the accumulation of gas and hence maintain the test pressure near atmospheric. Then the flow rate and inlet temperature were adjusted to the set conditions, and they

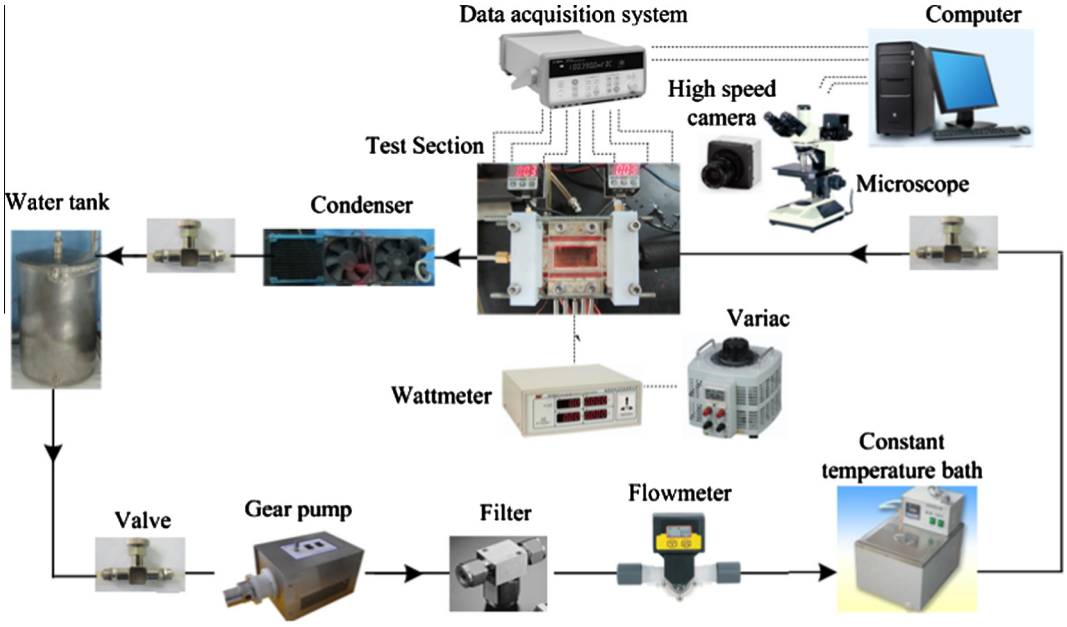

Fig. 2. Schematic of the flow boiling test system.

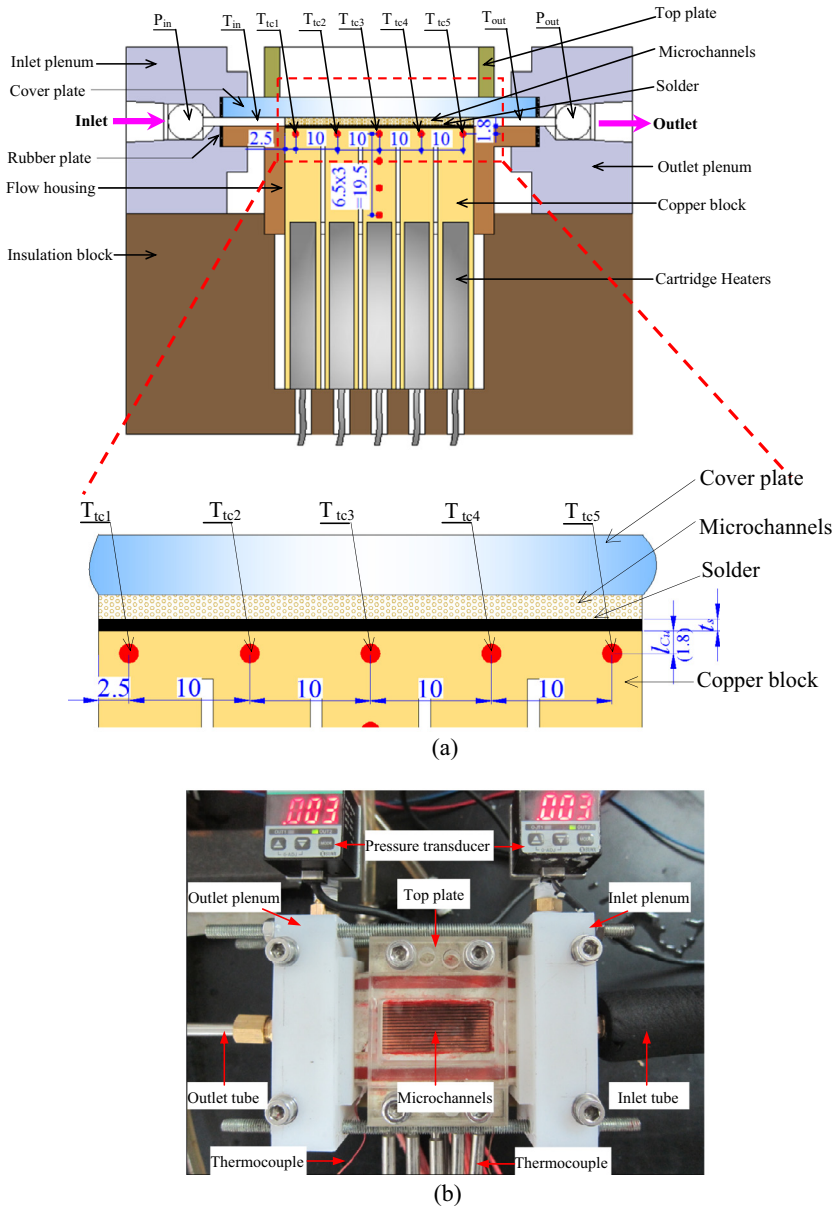

Fig. 3. Illustrations of test section: (a) schematic diagram; (b) photograph.

were kept constant throughout the test. The electrical power was supplied by the variac to the test section in a small increment of 15–30 W. After the system reached a steady state at each heat flux, all the measurements of temperatures, pressures and mass flow rate were collected at 1s interval for 2 min and averaged. Heat transfer coefficients were thus determined by using the averaged values from the measured data for 2 min.

2.3. Data reduction

Mass flux is referred as G and defined as

$$G = \dot{V}\rho/A_c \tag{3}$$

in which $\dot{V}$ is the volumetric flow rate, ρ is the fluid density, A_c is the cross-section area of the microchannels.

The effective heat flux is calculated from

$$q''_{eff} = q_{eff}/A_t \tag{4}$$

where A_t is the top platform area of the copper block, q_{eff} is the effective heat adsorption which follows $q_{eff} = \varphi Q$, with Q total electrical power input; φ is the ratio of the heat absorbed by the working fluid to the total input power. It is determined from a set of single-phase heat transfer experiments prior to boiling tests. The heat transfer ratio, φ, is found to range from 0.8 to 0.9 depending on flow rate and heat flux. Mean heat transfer ratio is utilized to calculate the effective heat power in the flow boiling cases, similar as other studies [3,9,10].

The local heat transfer coefficient is determined as follows,

$$h_{tp,tci} = \frac{q_{eff}}{\Delta T_{sat,tci} A_{ch}} \tag{5}$$

and

$$\Delta T_{sat,tci} = T_{w,tci} - T_{sat,tci} \tag{6}$$

where

$$T_{w,tci} = T_{tci} - q_{eff}\left(\frac{l_{Cu}}{k_{Cu}A_t} + \frac{l_{hs}}{k_{por}A_t} + \frac{t_s}{k_s A_t}\right) \tag{7}$$

where $\Delta T_{sat,tci}$ is the local wall superheat of the thermocouple location (tci, i = 1–5) and $T_{sat,tci}$ is the liquid saturation temperature. The wall temperature of porous microchannel ($T_{w,tci}$) is deduced from a thermal resistance network under the assumption of one-dimension heat conduction (see Ref. [20] for details), where T_{tci} is the measured temperatures in the copper block as depicted in Fig. 3, l_{Cu}, t_s and l_{hs} denotes the distance from the centre of thermocouple to the top heating surface of copper block, the thickness of solder paste, and the distance between the bottom surface of microchannels and the lowest line of the circular portion of reentrant cavity, respectively [20]. k_{Cu}, k_s and k_{por} are the thermal conductivities of copper, solder and porous matrix, respectively. The thermal conductivity of porous matrix, k_{por}, is measured to be 45 W/m K as follows: sintered porous specimens were prepared using the same copper powder and fabrication parameters as the present porous microchannels, and their porosities were the same as the porous microchannels. These specimens instead were measured using steady-state axial heat flow technique in dry conditions, which were conducted in a standard thermophysical property test system (Quantum Design Model PPMS-9). Though there may be small discrepancies between such measurements and the working conditions of reentrant porous microchannels, it is believed this can be thought to be negligible as the penetration of water into porous matrix was very limited as the permeability of porous matrix was in the order of 10^{-12} m^2 [20]. A_{ch} is the total heat transfer area of reentrant microchannels, which is given by the fin analysis method as follows,

$$A_{ch} = NL(P_{cir} + 2\eta H_{slot}) \tag{8}$$

where P_{cir} is the perimeter of the circular portion of each reentrant microchannel, N is the total number of reentrant microchannels, η is the fin efficiency as calculated as follows,

$$\eta = \frac{\tanh(mH_{slot})}{mH_{slot}} \tag{9}$$

in which m is the fin parameter as given by

$$m = \sqrt{\frac{h_{tp,tci} \cdot 2(L + W_{\mathrm{fin}})}{k_{por} L W_{\mathrm{fin}}}} \tag{10}$$

where W_{fin} is the width of the fin between two adjacent reentrant microchannels. The h_{tp} can thus be evaluated employing from Eqs. (5), (8), (9) and (10) with an iterative scheme.

The wall heat flux for reentrant porous microchannels is defined as

$$q''_{wall} = q_{eff}/A_{ch} \tag{11}$$

The vapor quality is calculated from an energy balance as follows [24,25],

$$x = \frac{1}{h_{fg}}\left(\frac{q_{eff}}{\dot{m}} \cdot \frac{L_i}{L} - C_p(T_{sat,tci} - T_{in})\right) \tag{12}$$

where h_{fg} is the latent heat of vaporization, L_i is the distance from the inlet to the thermocouple location. In the present study, the local two-phase heat transfer of the downstream thermocouple location (Z_{tc5}) near the exit of the channel is of primary focus.

The uncertainties in the microchannel geometry dimension are found to be within 7.7–8.9%. Uncertainties in individual temperature measurements are ±0.3 °C for the Type-K thermocouples. The measurement errors for the flow meter and pressure transducer are 2% and 0.1% of full scale, respectively. The uncertainty associated with the heating power supplied by the wattmeter is estimated to be 1%. Using the standard error analysis method [29], the uncertainties of vapor quality and two-phase heat transfer coefficient can be estimated to be in the range of 12.3–13.8%, 14.6–16.8%, respectively.

3. Results and discussion

3.1. Boiling curves

Fig. 4 shows the boiling curves of reentrant porous microchannels at different mass fluxes cases. The local wall temperature overshoot on the downstream thermocouple location near the exit (Z_{tc5}) is plotted versus the effective heat fluxes. The onset of nucleate boiling (ONB) is associated with a sudden change in the slope of the q''_{eff}–ΔT_{sat} curves. It can be noted that the reentrant porous microchannels can trigger the ONB at a small wall temperature overshoot, i.e., smaller than 1.5 °C. This can be attributed to that the porous matrix provides numerous active nucleate sites, and facilitates bubble embryos to grow and depart at a very low wall superheat [16,17]. After the ONB, the boiling curves of each RPMs at different mass fluxes nearly converged to a single line at the initial stage of boiling, implying that the heat dissipation was weakly dependant on the mass flux at this stage. This can be associated with the nucleate boiling dominant region, which accorded with the previous studies of solid microchannels [24,30]. With the heat fluxes increasing further, the boiling curves of different mass fluxes cases diverged, indicating that the influence of mass fluxes cannot be ruled out at moderate to high heat fluxes for all reentrant porous microchannels.

For these RPMs with different sizes, the sample RPM-D2 with the medium microchannel size presented a smallest increase in the wall temperatures with the increase of heat flux, and their boiling curves were steeper than the other two samples. This suggests that RPM-D2 presented the best heat transfer performance, which will be discussed in detail in the subsequent section.

3.2. Flow boiling heat transfer characteristics

In the present study, the local two-phase heat transfer coefficients of the most downstream thermocouple location (Z_{tc5}) near the outlet of microchannel are focused on as same as other studies [7,24,25,33], which relate to the greatest amount of saturated boiling and the largest vapor quality.

3.2.1. Effects of heat flux on two-phase heat transfer

Fig. 5 illustrates the local heat transfer coefficient as a function of heat flux and vapor quality. At the initial stage of boiling, the RPMs samples presented large h_{tp}. Since numerous microscopic pores inside the wall surface of porous microchannels provided perfect nucleation sites, it introduced large bubble growth and

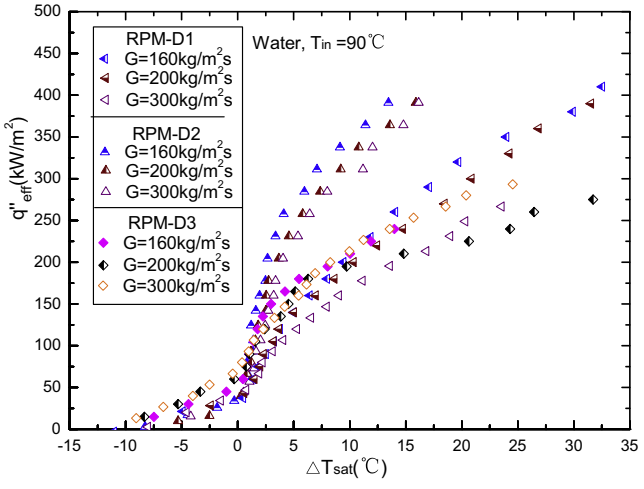

Fig. 4. Boiling curves of reentrant porous microchannels.

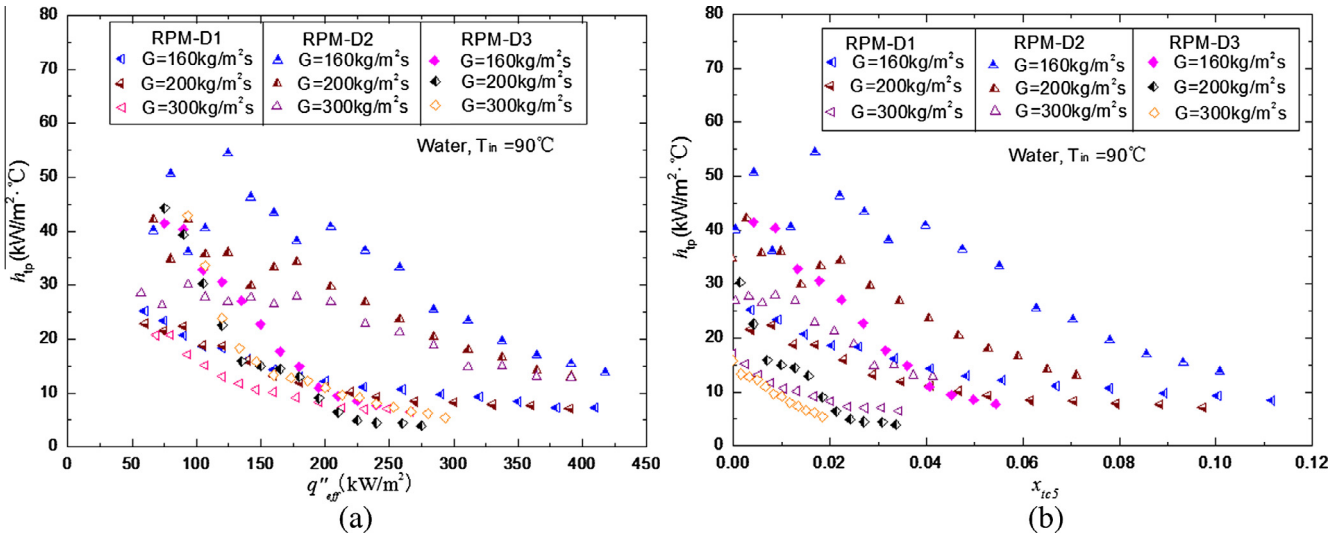

Fig. 5. Two-phase heat transfer coefficient of reentrant porous microchannels as a function of: (a) effective heat flux; (b) vapor quality.

departure frequencies after the onset of nucleate boiling, which resulted in a fast release of latent heat and thus resulted in a large h_{tp}. This stage was related to the nucleate boiling dominant region [31]. With the increase of heat flux as well as vapor quality, the two-phase heat transfer coefficient tended to decrease. This trend accorded with other water boiling tests with solid copper or silicon microchannels [7,28]. This region can be linked to the forced convective boiling dominant region, as the increase of heat flux played an adverse role of on the h_{tp}, and the vapor quality exerted a notable influence on the heat transfer performance. The contribution from convective boiling heat transfer began to dominate in the heat transfer process. The churn flow and annular flow were found to govern in the microchannels, and the heat fluxes were dissipated mainly via the thin film evaporation. From the above, one can note that the heat flux play a notable role on two-phase heat transfer performance of RPMs.

3.2.2. Effects of mass flux on two-phase heat transfer

In the present study, three test cases with the mass fluxes ranged from 160 to 300 kg/m^2 s were conducted under the high inlet temperatures (T_{in} = 90 °C), and the saturated boiling heat transfer performance were focused on. From Fig. 5, one can note that except the nucleate boiling regions after the ONB of RPM-D2, the two-phase heat transfer performance of reentrant porous microchannels presented a weak dependence on the mass fluxes, i.e., it showed a slight decrease in h_{tp} with the increase of mass fluxes. Possible reason may be that at a given heat flux, the vapor quality decreased with the increase of mass fluxes, which may introduce thinner liquid film around the vapor core in the annular flow, thereby the dry-out of liquid film occurred more rapidly and resulted in a smaller heat transfer performance[32]. Such surprising behaviors have been also observed in the water boiling tests in solid copper microchannels [33,34], and the refrigerants (R134a, R-245fa) boiling tests in copper microchannels [35].

3.2.3. Effects of microchannel size on two-phase heat transfer

From Fig. 5, one can note that the small sample RPM-D1 presented the worst heat transfer coefficients in the early stage at nucleate boiling region. This was associated with its smallest wall surface area, which resulted in less bubble nucleation sites. The other two samples with large size presented a much higher h_{tp} than RPM-D1. With the increase of heat fluxes and vapor qualities, all the reentrant porous microchannels exhibited a deterioration in heat transfer rates. At moderate and high heat fluxes conditions, the RPM-D2 with the medium hydraulic diameter presented the largest h_{tp}, i.e., it exhibited a 2–3 folds enhancement in two-phase heat transfer rate compared to the other two samples. It seems that the boiling heat transfer of reentrant porous microchannels did not show a monotonic dependence on the channel size. The above effects of channel size on the flow boiling heat transfer of RPMs can be also verified by the elimination of the difference of heat transfer surface area of channel wall, as shown in Fig. 6, where the h_{tp} was plotted with respect to the wall heat fluxes. Such trend differed from many previous studies of solid rectangular microchannels or circular ducts [16,36–38] considerably, in which enhanced heat transfer can be reached by decreasing the channel size.

The above different heat transfer behaviors of three reentrant porous microchannels can be linked to the microchannel size effects on the boiling flow patterns. As mentioned above, stable bubbly flow dominated at the beginning of boiling process for reentrant porous microchannels. For the small sample RPM-D1, the bubble ebullition and expansion were restricted by the limited space inside the microchannels, thus the bubbles were usually of

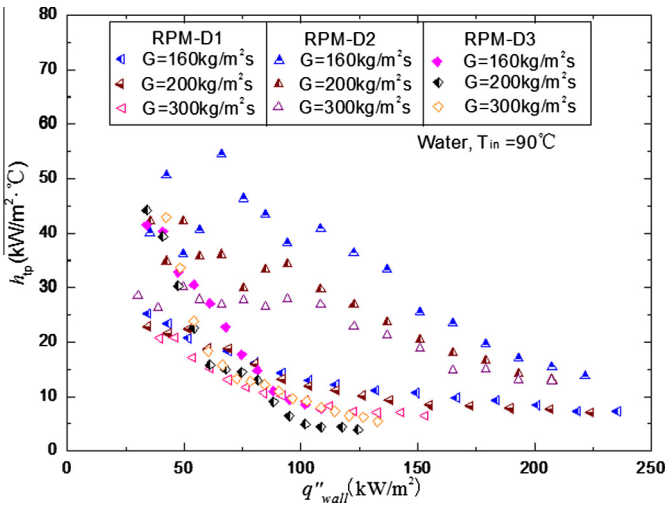

Fig. 6. Two-phase heat transfer coefficient as a function of wall heat fluxes for reentrant porous microchannles.

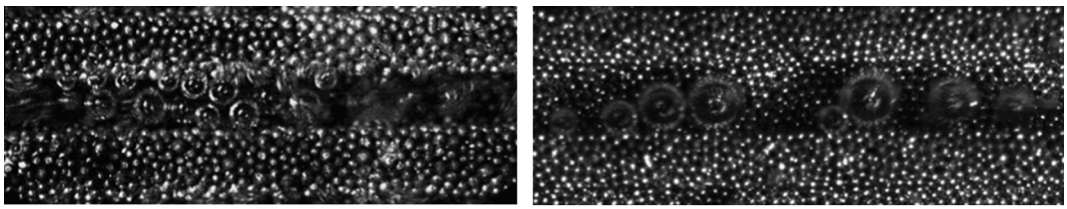

Fig. 7. Bubbly flow in the reentrant porous microchannels: (a) RPM-D1, T_{in} = 90 °C, G = 160 kg/m^{2}s, q''_{eff} = 60 kW/m^2; (a) RPM-D2, T_{in} = 90 °C, G = 160 kg/m^{2}s, q''_{eff} = 67 kW/m^2.

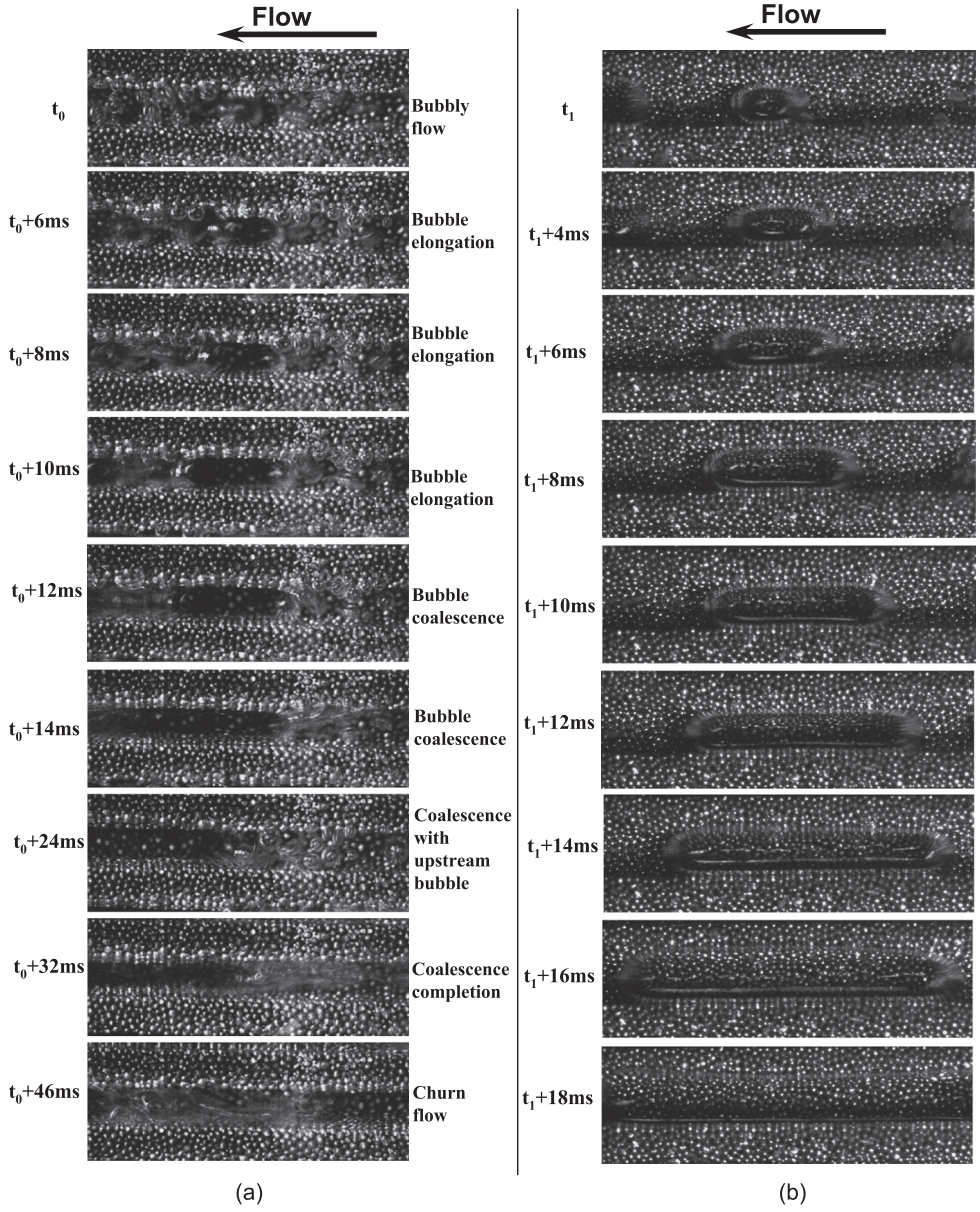

Fig. 8. (a) Rapid transition of flow pattern from bubbly flow to churn flow in sample RPM-D1 at T_{in} = 90 °C, G = 200 kg/m^{2}s, q''_{eff} = 105 kW/m^2; (b) bubble elongation of sample RPM-D2 at T_{in} = 90 °C, G = 200 kg/m^{2}s, q''_{eff} = 160 kW/m^2.

small size, as shown in Fig. 7(a). Nevertheless, for the other two samples with large size, the bubbles could grow to a large size as there was enough space for their expansion, as illustrated in Fig. 7(b). Furthermore, RPM-D1 induced an early and rapid coalescence of bubbles just after it grew and departed into the microchannels under the strong confinement effect of microchannel wall and narrow slot. It introduced an early transition from bubbly flow to elongated flow or churn flow, and very short period of bubbly flow only existed just after the ONB. Fig. 8(a) illustrates the rapid transition of bubbly flow to churn flow in RPM-D1 at mass fluxes of 200 kg/m^{2}s, and heat fluxes of 105 kW/m^2, which completed within a very short period (less than 50 ms). This

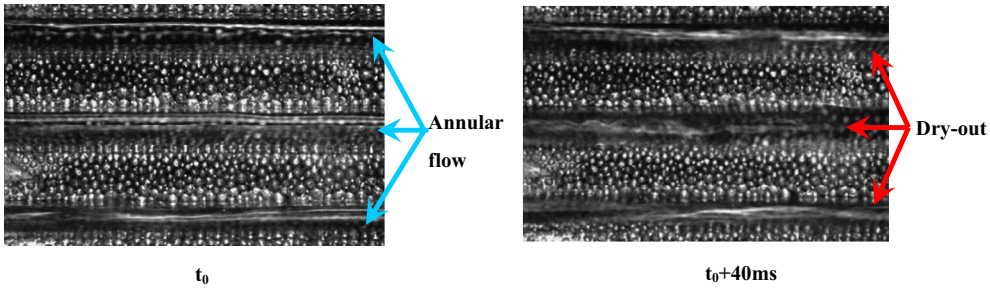

Fig. 9. Periodic alternations of annular flow and partial wall dry-out in the microchannels of sample RPM-D1 at T_{in} = 90 °C, G = 200 kg/m^{2}s, q''_{eff} = 240 kW/m^2.

suppressed the nucleate boiling activities and reduced the two-phase heat transfer. Therefore, early deterioration of heat transfer was noted for sample RPM-D1. For other two large samples RPM-D2 and RPM-D3, the bubbly flow and elongated bubbly flow (slug flow) lasted for a much longer time than RPM-D1. Fig. 8(b) illustrates the bubble elongation process of RPM-D2 at G = 200 kg/m^{2}s, q''_{eff} = 160 kW/m^2, in which the bubble expansion occurred much later than the RPM-D1 due to its less intense wall confinement. With the heat flux and vapor quality increasing, it was found that the churn flow and annular flow dominated at lower heat fluxes in the microchannels of RPM-D1 than in the large microchannels, which suppressed the nucleate boiling earlier significantly. At the stage of high heat fluxes, periodic alternations of annular flow and partial wall dry-out can be observed in the small microchannels, as illustrated in Fig. 9. This resulted in the further deterioration in heat transfer performance and a very small h_{tp} can be noted for RPM-D1. Such early establishment of annular flow and partial wall dry-out in smaller microchannels were also reported in the previous studies of solid rectangular microchannels [23,25]. On the other side, for the sample RPM-D3 with large channel size, the liquid film formed between the vapor core and microchannel wall surface may be much thicker than the other two samples due to its largest circular cavities, which resulted in higher thermal resistance. Since the heat fluxes in the forced covective boiling region were mainly transported via thin film evaporation, a fast deterioration in h_{tp} can be noted for RPM-D3 due to the much weaker thin film evaporation. For the RPM-D2 with the medium size, it may reach a good balance and exhibited moderate liquid film thickness, while simultaneously hindered the occurrence of early partial wall dryout, therefore it presented the largest h_{tp}. It was found that the churn flow and annular flow persisted to high heat fluxes for RPM-D2, and the heat transfer declined gradually. Therefore, it presented the best heat transfer performance at moderate to high heat fluxes.

3.3. Two-phase flow instabilities

Unstable boiling with two-phase flow instabilities is commonly encountered in the flow boiling conditions of microchannels, which can be mitigated by installing inlet restrictors in the upstream of test section [39]. In the present study, in order to examine the microchannel size effect on the two-phase flow instability behavior of the reentrant porous microchannels, no inlet restrictors were installed. Fig. 10 shows typical fluctuation curves of inlet pressure of there RPMs samples, in which the standard deviations (σ) in P_{in} were also shown in the figures. It was found that long period and larger amplitude of inlet pressure oscillations (1.5–3 kPa) occurred in RPM-D1, whereas the other two large RPMs presented mild flow instabilities. The RPM-D1 with small size presented a much larger magnitude of fluctuation in the inlet pressure, i.e., the standard deviations (σ) in P_{in} of RPM-D1 were 1–3 times higher than the other two samples. For the small sample

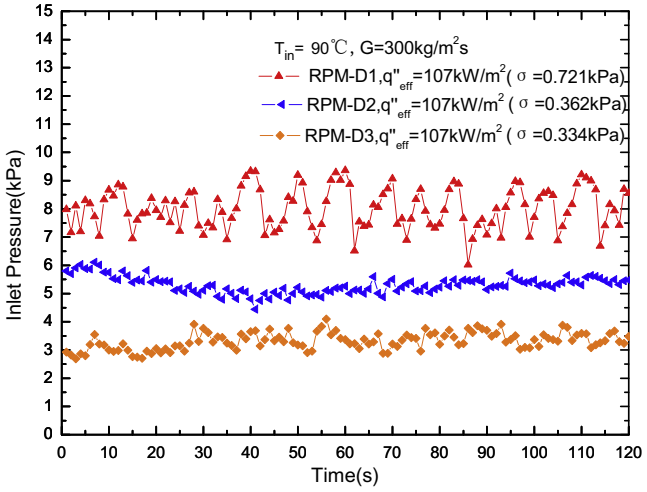

Fig. 10. Variation of inlet pressure of reentrant porous microchannels at T_{in} = 90 °C, G = 300 kg/m^{2}s.

RPM-D1, due to the limited room and strong confinement effect of wall surface, the growth of tiny bubbles was restricted and they can only expand upstream and downstream. This induced easy coalescence of adjacent bubbles in the stream-wise direction and elongated long bubbles formed. Local pressures in the microchannels increased sharply and pushed the upstream bubbles to flow reversely even into the inlet plenum. A high inlet pressure was thus obtained. With the accumulation of incoming liquid, the inlet pressure increased to an enough large value to overcome the local pressures in the microchannels. The vapor flows were then pushed out of the microchannels and induced the decrease of inlet pressures. While for the other two samples with large microchannel size, the large circular cavities provided enough space to accommodate more discrete bubbles, which reduced the chance of bubble coalescence. They facilitated the bubble movement along the stream-wise direction, and the flow reversal was much less notable. Therefore, much smaller magnitude of fluctuation of inlet pressure was noted for the two large reentrant porous microchannels, and they were able to sustain fairly stable boiling process even though no inlet restrictors were installed.

4. Conclusions

In this study, reentrant porous microchannels with different sizes were fabricated for two-phase heat sink cooling systems. Flow boiling experiments of water were performed under different mass fluxes. The effects of heat flux, mass flux and microchannel size on flow boiling performance of reentrant porous microchannels were examined. It was found that the sintered porous microchannels

promoted the bubble nucleation and presented a small wall superheat for onset of nucleate boiling. The two-phase heat transfer performances of RPMs were strongly dependent on the heat flux, but presented a weak dependence on the mass flux. The reentrant porous microchannels with the medium size presented superior heat transfer performance compared to the other two samples at moderate to high heat fluxes, i.e., a 2–3 folds enhancement in two-phase heat transfer rate was reached. The RPMs with small size induced a rapid transition from bubbly flow to slug and churn flow due to the limited space and strong confinement effect. This caused the early deterioration of heat transfer performance and also resulted in unstable boiling with large magnitude of flow oscillation. Two large RPMs were found to facilitate the mitigation of two-phase flow instabilities. The above results highlight the microchannel size effect on the flow boiling behaviors of reentrant porous microchannels, and suggest that such type of microchannels with the medium size may be favorable for the efficient cooling of microelectronic devices.

Acknowledgements

The research was financially supported under the Grants of the National Nature Science Foundation of China No. 51405407 and No. 51275180, Basic research projects of Shenzhen research & development fund No. JCYJ20140417161915014 , and the program No. 2014EP0012 from the Open Fund of Key Laboratory of E&M (Zhejiang University of Technology), Ministry of Education & Zhejiang Province.

References

[1] D.B. Tuckerman, R.F.W. Pease, High-performance heat sinking for VlSI, IEEE Electron Dev. Lett. 2 (1981) 126–129.
[2] B. Agostini, M. Fabbri, J.E. Park, L. Wojtan, J.R. Thome, B. Michel, State of the art of high heat flux cooling technologies, Heat Transfer Eng. 28 (2007) 258–281.
[3] G. Hetsroni, A. Mosyak, Z. Segal, G. Ziskind, A uniform temperature heat sink for cooling of electronic devices, Int. J. Heat Mass Transfer 45 (2002) 3275–3286.
[4] F.J. do Nascimento, H.L.S.L. Leão, G. Ribatski, An experimental study on flow boiling heat transfer of R134a in a microchannel-based heat sink, Exp. Thermal Fluid Sci. 45 (2013) 117–127.
[5] A.D. Sommers, K.L. Yerkes, Using micro-structural surface features to enhance the convective flow boiling heat transfer of R-134a on aluminum, Int. J. Heat Mass Transfer 64 (2013) 1053–1063.
[6] P.M.-Y. Chung, M. Kawaji, The effect of channel diameter on adiabatic two-phase flow characteristics in microchannels, Int. J. Multiphase Flow 30 (2004) 735–761.
[7] W. Qu, I. Mudawar, Flow boiling heat transfer in two-phase micro-channel heat sinks—I. Experimental investigation and assessment of correlation methods, Int. J. Heat Mass Transfer 46 (2003) 2755–2771.
[8] Y. Wang, K. Sefiane, S. Harmand, Flow boiling in high-aspect ratio mini- and micro-channels with FC-72 and ethanol experimental results and heat transfer correlation assessments, Exp. Thermal Fluid Sci. 36 (2012) 93–106.
[9] J. Xu, Y. Gan, D. Zhang, X. Li, Microscale boiling heat transfer in a micro-timescale at high heat fluxes, J. Micromech. Microeng. 15 (2005) 362–376.
[10] H.Y. Wu, P. Cheng, Visualization and measurements of periodic boiling in silicon microchannels, Int. J. Heat Mass Transfer 46 (2003) 2603–2614.
[11] S.G. Kandlikar, W.K. Kuan, D.A. Willistein, J. Borrelli, Stabilization of flow boiling in microchannels using pressure drop elements and fabricated nucleation sites, ASME J. Heat Transfer 128 (2006) 389–396.
[12] C.N. Ammerman, S.M. You, Enhancing small-channel convective boiling performance using a microporous surface coating, ASME J. Heat Transfer 123 (2001) 976–983.
[13] V. Khanikar, I. Mudawar, T. Fisher, Effects of carbon nanotube coating on flow boiling in a micro-channel, Int. J. Heat Mass Transfer 52 (2009) 3805–3817.
[14] A.K.M.M. Morshed, T.C. Paul, J. Khan, Effect of Al_2O_3 nanoparticle deposition on flow boiling performance of water in a microchannel, Exp. Thermal Fluid Sci. 47 (2013) 6–13.
[15] Z. Zhao, R.A. Wirtz, Flow-through boiling of isopentane in structured-porous fins effects of system parameters, ASME J. Heat Transfer 134 (2012) 071501.
[16] Y. Sun, L. Zhang, H. Xu, X. Zhong, Flow boiling enhancement of FC-72 from microporous surfaces in minichannels, Exp. Thermal Fluid Sci. 35 (2011) 1418s–1426.
[17] P. Bai, T. Tang, B. Tang, Enhanced flow boiling in parallel microchannels with metallic porous coating, Appl. Therm. Eng. 58 (2013) 291–297.
[18] A. Kosar, C. Kuo, Y. Peles, Boiling heat transfer in rectangular microchannels with reentrant cavities, Int. J. Heat Mass Transfer 48 (2005) 4867–4886.
[19] C.J. Kuo, Y. Peles, Local measurement of flow boiling in structured surface microchannels, Int. J. Heat Mass Transfer 50 (2007) 4513–4526.
[20] D. Deng, Y. Tang, D. Liang, H. He, S. Yang, Flow boiling characteristics in porous heat sink with reentrant microchannels, Int. J. Heat Mass Transfer 70 (2014) 463–477.
[21] S. Saitoh, H. Daiguji, E. Hihara, Effect of tube diameter on boiling heat transfer of R-134a in horizontal small-diameter tubes, Int. J. Heat Mass Transfer 48 (2005) 4973–4984.
[22] M. Lee, L.S.L. Cheung, Y. Lee, Y. Zohar, Height effect on nucleation-site activity and size-dependent bubble dynamics in microchannel convective boiling, J. Micromech. Microeng. 15 (2005) 2121–2129.
[23] J. Lee, I. Mudawar, Fluid flow and heat transfer characteristics of low temperature two-phase micro-channel heat sinks – Part2: subcooled boiling pressure drop and heat transfer, Int. J. Heat Mass Transfer 51 (2008) 4327–4341.
[24] T. Harirchian, S.V. Garimella, Microchannel size effects on local flow boiling heat transfer to a dielectric fluid, Int. J. Heat Mass Transfer 51 (2008) 3724–3735.
[25] T. Harirchian, S.V. Garimella, The critical role of channel cross-sectional area in microchannel flow boiling heat transfer, Int. J. Multiphase Flow 35 (2009) 904–913.
[26] S.G. Singh, A. Kulkarni, S.P. Duttagupta, B.P. Puranik, A. Agrawal, Impact of aspect ratio on flow boiling of water in rectangular microchannels, Exp. Therm. Fluid Sci. 33 (2008) 153–160.
[27] B. Fu, C. Lee, C. Pan, The effect of aspect ratio on flow boiling heat transfer of HFE-7100 in a microchannel heat sink, Int. J. Heat Mass Transfer 58 (2013) 53–61.
[28] G. Wang, P. Cheng, A.E. Bergles, Effects of inlet/outlet configurations on flow boiling instability in parallel microchannels, Int. J. Heat Mass Transfer 51 (2008) 2267–2281.
[29] J.R. Taylor, An Introduction to Error Analysis, second ed., University Science Books, 1997.
[30] D. Liu, S.V. Garimella, Flow boiling heat transfer in microchannels, ASME J. Heat Transfer 129 (2007) 1321–1332.
[31] M.E. Steinke, S.G. Kandlikar, An experimental investigation of flow boiling characteristics of water in parallel microchannels, ASME J. Heat Transfer 126 (2004) 518–526.
[32] S. In, S. Jeong, Flow boiling heat transfer characteristics of R123 and R134a in a micro-channel, Int J Multiphase Flow 35 (2009) 987–1000.
[33] E. Sobierska, R. Kulenovic, R. Mertz, M. Groll, Experimental results of flow boiling of water in a vertical microchannel, Exp. Therm. Fluid Sci. 31 (2006) 111–119.
[34] E. Galvis, R. Culham, Measurements and flow pattern visualizations of two-phase flow boiling in single channel microevaporators, Int. J. Multiphase Flow 42 (2012) 52–61.
[35] S.S. Bertsch, E.A. Groll, S.V. Garimella, Effects of heat flux, mass flux, vapor quality, and saturation temperature on flow boiling heat transfer in microchannels, Int. J. Multiphase Flow 35 (2009) 142–154.
[36] C. Martın-Callizo, B. Palm, W. Owhaib, Subcooled flow boiling of R-134a in vertical channels of small diameter, Int. J. Multiphase Flow 33 (2007) 822–832.
[37] Y. Wang, K. Sefiane, Effects of heat flux, vapour quality, channel hydraulic diameter on flow boiling heat transfer in variable aspect ratio micro-channels, Int. J. Heat Mass Transfer 55 (2012) 2235–2243.
[38] C.A. Chen, W.R. Chang, K.W. Li, Y.M. Lie, T.F. Lin, Subcooled flow boiling heat transfer of R-407C and associated bubble characteristics in a narrow annular duct, Int. J. Heat Mass Transfer 52 (2009) 3147–3158.
[39] W. Qu, I. Mudawar, Transport phenomena in two-phase micro-channel heat sinks, ASME J. Heat Transfer 126 (2004) 213–224.